ISSN 0029 - 3865

CBPF-NF-005/90

FIRETUBE MODEL AND PROTON-NUCLEUS COLLISION

by

R.A.M.S. NAZARETH[1], R. DONANGELO[1],
T. KODAMA and S.B. DUARTE

Centro Brasileiro de Pesquisas Físicas - CBPF/CNPq
Rua Dr. Xavier Sigaud, 150
22290 - Rio de Janeiro, RJ - Brasil

[1]Instituto de Física
Universidade Federal do Rio de Janeiro
21945 - Rio de Janeiro, RJ - Brasil

Abstract

The firetube model of hadron-hadron collision process is extended to describe proton-nucleus collisions at ultrarelativistic energies. According to the model, nucleon-nucleon firetubes created by the interaction between the nucleon projectile and the wounded target nucleons contribute additively for the energy density of a resultant effective firetube. We calculate the rapidity distributions for α-p for $\sqrt{s_{nn}}$=44 GeV and for p-Ar and p-Xe at 200 GeV incident energy. The results are in good agreement to the experimental data. We also discuss the possibility of applying the model to light nucleus-nucleus collisions and show the results for $\alpha - \alpha$ collision at $\sqrt{s_{nn}}$=30 GeV.

Key-words: P-nucleus collision; Firetube model.

I. Introduction

It is more than a decade since Quantum Chromodynamics (QCD) gained general acceptance among physicists as the theory of strong interactions between hadrons. Many experimental and theoretical evidences indicate strongly that this belief is a correct one. However, due to the lack of mathematical tools to manage the nonlinear and nonperturbative aspects of the theory, one can present very little theoretical model independent descriptions for the most interesting phenomena of hadron interactions such as multiple particle production processes.

From the experimental side, ultra-relativistic nucleus-nucleus collisions are expected to furnish a sound basis of the QCD if a clear signature of the formation of a quark-gluon plasma (QCP) is observed[1,2]. We may classify many proposed signatures roughly into two categories. In one the effects of QGP appear as changes in some elementary processes and in the other the dynamical quantities are directly measured to establish the thermodynamical relationship manisfesting the existence of the expected phase transition. Strange particle production and J/ψ supression belong to the former type and the $P_T - dn/dy$ diagram belongs to the latter. Unfortunately, the present experimental data at CERN and BNL are not conclusive with respect to the formation of the QGP. This is basically due to the very complicated initial and final state interactions among the produced hadrons which average out the information from the intermediate high energy density states. It may also be true that the present experimental situation corresponds to the mixed phase where a clear signature of the phase transition can hardly be expected.

A microscopic description of the whole process of nucleus- nucleus collision starting from QCD is not available at this moment. This is also the case even in the simpler proton-proton collision case. Thus, we have to rely on models. There are now several models of multiple particle production in hadron-hadron collision processes. ΩWhile no theory describing nucleus-nucleus collisions at relativistic energies is available, the best thing we can do is to apply these proton-proton models to the nucleus case by considering simple extrapolation of nucleon-nucleon collisions[3−8]. One expects that the difference, if any, between quantities calculated in this way and experimental data could indicate many body or collective effects, provided that the treatment of proton-proton collisions is reliable enough. The first step to be done in this direction is of course to study proton-nucleus collisions.

Hadron-Nucleus interactions at ultra-relativistic incident energies are now available from many sources in the literature[9,10]. One of the interesting features of these data is the behaviour of the rapidity distribution in the projectile fragmentation region. In the mid and low rapidity regions, the rapidity distribution increases significantly with the target mass number, but the behaviour in the highest rapidity region is almost independent of target size, *i.e.*, it falls to zero in almost exactly the same way as in the proton-proton case. This behaviour was discussed by many authors and one interpretation is to suppose that the incident proton, even after several nucleon-nucleon collisions is always accompanied by a string which is identical to that of a single nucleon-nucleon collision. Therefore, the high rapidity hadrons produced from this string have the same properties as those of a single nucleon-nucleon collision.

This picture seems to be supported by the experimental systematics of the multiplicity.

One finds that the average multiplicity of $p-A$ collision is given by

$$< n_{p-A} >= \frac{1}{2}(\nu+1) < n_{p-p} >, \tag{1}$$

where ν is the mean number of collisions that the incident nucleon suffers inside the target, $< n_{p-p} >$ is the average multiplicity for a proton-proton collision. Eq.(1) may be interpreted by saying that in each nucleon-nucleon collision, one target-like half string is produced, while a single projectile-like half string is formed, and all these half-strings contribute to the final hadron spectra indeppendently.

On the other hand, there exists another possibility to explain the behaviour of the rapidity distribution in the fragmentation region. For proton-nucleus collisions, there always exist contributions from nucleon-nucleon collisions near the edge of the target nucleus which are essentially identical to free nucleon-nucleon collisions. Therefore, we may expect that the properties of particle spectra in the high rapidity region are just a reflection of nuclear surface effects. As for the systematics of multiplicities, we note that the contribution of multiple scatterings in the target nucleus in the low rapidity region may not be well estimated. There might exist a room for other mechanisms which give a similar dependence of the average multiplicity as a function of target mass.

Recently, two of the present authors (R.A.M.S.N.,T.K.) proposed a simple phenomenological model for the proton-proton collision process[11-13] based on a mechanism in which a chromodynamical firetube fragments into intermediate fireballs which subsequently decay into the observed hadrons. This model was found to reproduce the experimental rapidity distribution within a wide energy interval, extending from $\sqrt{s} \sim 20GeV$ to $\sqrt{s} \sim 1TeV$. The advantage of this model when applied to the proton-nucleus or nucleus-nucleus collision is due to its simplicity and also to the fact that nucleon-nucleon collision geometry is explicitly taken into account. The model assumes a formation of a firetube which has cross section determined by the overlap of two nucleons. The natural extension of this model to the many nucleon case is to consider that firetubes generated by several nucleon-nucleon collisions fuse into a thicker one.

In this article, we apply the firetube model for proton-nucleus collisions according to the above idea in order to calculate the observed particle spectra. For simplicity, we consider only pions as secondary particles.

In the following section, we review briefly the firetube model, and in § *III*, we describe how to apply the model to the case of a proton-nucleus collision. We discuss the possible extention to the nucleus-nucleus case, although in this last case, the effects of final state interactions could be more important.

II. Effective string model of p-p collisions.

The phenomenological model developed in refs.[11-13] describes proton-proton collisions as a three-stage process. In the first part of the collision the protons become colored objects due to exchange of sea quarks, generating a chromodynamical flux tube between them. In the following stage this tube fragments into a set of intermediate mass objects (fireballs), which subsequently decay into the observable hadrons. This model is similar to the one developed by the Lund group[14], except that in the latter hadrons are produced directly from fragmentation of the effective string, without an intermediate fireball stage[15]. In what follow we briefly present the main ingredients of the model and introduce some improvements on the description of the fireball decay process.

The tension coefficient for the effective string is given by

$$k_{eff} = \epsilon_0 \, A(b) \,, \tag{2.1}$$

where ϵ_0 is the volumetric energy density of the flux tube of transverse area $A(b)$. The transverse area of the effective string is proportional to the total proton-proton cross section times an universal function of the impact parameter b,[13]

$$A(b) = \sigma_{tot}(\sqrt{s}) \; f(b) \,. \tag{2.2}$$

The motion of the two colored proton residues is obtained from the classical Hamiltonian

$$H(b) = (p_1^2 + m_p^2)^{1/2} + (p_2^2 + m_p^2)^{1/2} + k_{eff} \mid x_1 - x_2 \mid , \tag{2.3}$$

where x_i, p_i are the coordinates and momenta of the particles at each end of the effective string. The time evolution of the system is obtained by solving the equations of motion derived from the Hamiltonian (2.3). The trajectories of the end-point particles are two intertwined hyperbolas that may be approximated by zigzag lines if the mass of the residues can be neglected in comparison with the total energy[13].

Another basic ingredient of the model is the stochastic $q, \bar{q}$ creation at any point of the effective string between the two end particles. This pair creation process splits the original string into two substrings, their energy and momentum being determined by the precise point where the break took place. Pair creation may continue within the substrings and we consider that the string breaking sequence continues until, due to the chromodynamic field, each effective substring collapses into a point, thereby converting its kinetic energy into internal energy of a highly excited object (fireball). In ref. 13 are given additional details of the string break-up process as well as the resulting fireball mass and rapidity distributions, which we quote below for completeness.

If we let w be the probability of string breaking per unit time, M the initial center of mass energy, m and y the fireball mass and rapidity, then the end-point fireball distribution, in the limit $M \gg m_p$, is given by

$$\left[\frac{d^2P}{dm\,dy}\right]_{EP} = \frac{mw}{k_{eff}^2} \, exp\left[-\frac{wmM}{2k_{eff}^2} e^{\mp y}\right] \Theta(\mp y + y_{max}) \tag{2.4}$$

where the minus and plus signs of y refer to the fireball from the right and left, respectively, $y_{max} = \ln(M/m)$, and Θ is the Heavyside function. For the non-end-point case we have, in the same limit,

$$\left[\frac{d^2P}{d\overline{m}\,dy}\right]_{NEP} = 2\overline{m}\,[E_1(wM^2/2k^2) - E_1(\overline{m}^2 e^{y_{max}-y}) - E_1(\overline{m}^2 e^{y_{max}+y}) - E_1(\overline{m}^2)]\,\Theta(y_{max}^2 - y^2) \tag{2.5}$$

where $E_1(x)$ is the exponential integral function and $\overline{m} = m\sqrt{w/2k^2}$.

In the final stage of the model the hadron spectrum is calculated from the decay of the fireballs. Several alternative assumptions may be made to treat this decay. In Ref.[13] a statistical thermal model was considered. According to it the pion spectrum from the decay of a fireball with mass m_f and rapidity y_f is given by

$$\frac{1}{\sigma_\pi}\frac{d^3\sigma_\pi}{dp^3} = \frac{A}{\pi}\, e^{-E_t \cosh(y-y_f)/T(m_f)} \tag{2.6}$$

where $E = E_t \cosh(y - y_f)$ and p are the energy and momentum of the emitted pions and A a normalization constant. From the distribution (2.6) the pion rapidity, pseudorapidity and transverse momentum distributions can be obtained in a simple way[13]. Although the rapidity and pseudorapidity distributions, and consequently the pion multiplicity calculated with the thermal decay model agree well with data, the model predicts large values for the transverse momentum compared to the experimental data. This overestimate of transverse momentum may be attributed to the isotropic nature of fireball decay. According to the Landau picture, even after attaining a local equilibrium when a substring collapses into a point, the resultant fireball expands londitudinally due to the Lorentz contraction effect. Therefore, in order to improve the transverse momentum distribution of the model without affecting the other properties we include in this work the longitudinal hydrodynamical expansion for the fireball decay process.

According to Ref.16, the effect of longitudinal expansion of a fireball can be approximately expressed in terms of a Gaussian rapidity distribution of the fluid elements of the fireball. Thus, the final hadron spectra is obtained as a convolution of the fluid motion and the thermal decay spectra of hadrons. Using this fact eq.(2.6) becomes

$$\frac{1}{\sigma_\pi}\frac{d^3\sigma_\pi}{dp^3} = \frac{A}{\pi}\int_{-\infty}^{+\infty} d\overline{y} e^{-\alpha(\overline{y}-y_f)^2}\, e^{-E_t \cosh(y-\overline{y})/T(m_f)} \tag{2.7}$$

where $\overline{y}$ stands for the rapidity of the fluid element and α is a parameter related to the longitudinal energy of the fluid in the fireball. For large α we recover the isotropic decay inclusive spectrum of eq.(2.6). For a given m, T and the average multiplicity $\bar{N}$, the value of α is determined by the normalization condition,

$$\int d^3\vec{p}\,\frac{1}{\sigma_\pi}\,\frac{d^3\sigma_\pi}{dp^3} = \bar{N} \tag{2.8}$$

and

$$\int d^3\vec{p}\,\frac{E}{\sigma_\pi}\,\frac{d^3\sigma_\pi}{dp^3} = m \tag{2.9}$$

The average multiplicity of a fireball decay is also determined in accordance with the hydrodynamical model ($\bar{N} = 2.2\sqrt{m}$). However, for small values of $m(m < 1\ GeV)$ for which the above three conditions give a negative value of α, we assume the isotropic decay.

The temperature T of a fireball as a function of its mass is calculated by the following function,

$$T = \frac{0.16}{1 - 1.6v} \tag{2.10}$$

where

$$v = \frac{1.2\,(m^{1/7} - 1)}{m^{1/7} + \sqrt{m^{2/7} - 2.24(m^{1/7} - 1)}} \tag{2.11}$$

which simulates the behaviour of the transverse momentum $< p_T >$ as a function of the fireball mass[17], $< p_T > \sim m^{1/7}$.

With the above prescription for the decay of a fireball, we can calculate the final hadron spectra folding the fireball mass distribution with the fireball decay. In Fig.1, we plotted the calculated $< p_T >$ as a function of the incident energy which shows an excellent agreement with the experimental data[18-20]. Note that the slow increase of $< p_T >$ for higher energies reflects the increase of the average fireball mass.

The calculation of the rapidity distribution and multiplicity of the pions produced in the collision is similar to the one performed for the isotropic case in ref. 13, and therefore we omit it here. In the next section we apply the description of the p-p collision developed here to the proton-nucleus case.

III. Proton-Nucleus Collisions

3.1 The Model

A straightforward application of the firetube model to proton-nucleus collisions is as follows:

For a given impact parameter $\vec{b}$, the projectile nucleon n_p moves through the target nucleus on a straight line and interacts with every target nucleons n_t which satisfy the condition,

$$\sigma_{nn} \geq \pi \left|\vec{b} - \vec{s}_i\right|^2 \tag{3.1}$$

where σ_{nn} is the total inelastic nucleon-nucleon cross-section and s_i is the transversal coordinates of the i-th target nucleon. For each collision a firetube with energy density k_i is formed according the overlap area between n_p and n_t as described in § II.

These independent firetubes are assumed to fuse into an effective firetube. We assume that all the nucleon-nucleon firetubes contribute additively for the energy density of this resultant effective firetube with $k = \sum_i^{\nu} k_i$, where ν is the number of wounded nucleons. The additivity of the firetubes into a single effective firetube reflects the idea that the energy density of a firetube is essentially proportional to the number of excited sea partons.

Thus, a thick effective firetube is formed between the incident nucleon and a massive object formed by the ν wounded nucleons in the target. We desregard the internal dynamics of this massive object. The Hamiltonian of the system is

$$H(b) = \sqrt{p_1^2 + m_n^2} \; + \; \sqrt{p_2^2 + M^2} \; + \; k\,|x_1 - x_2| \tag{3.2}$$

where (x_1, p_1) and (x_2, p_2) are the coordinates and momenta of the two massive end points, m_n is the nucleon mass and M is the end point mass corresponding to the energy of the system of ν wounded nucleons. Taking into account the spatial separation among the wounded nucleons we take approximately

$$M = \sum_{i=1}^{\nu} m_i \; + \; E^* \tag{3.3}$$

with $E^* = \sum_{i=1}^{\nu} k_i \mid z_i - z_f \mid$ where z_i is the z coordinate of the i-th wounded nucleon and z_f is that of the last wounded nucleon (Fig.2).

After these assumptions, we follow the dynamics of the effective firetube in a similar way to the proton-proton case to calculate the final hadron spectra. The other model parameters, e.g., those for fragmentation mechanism are taken to be the same as in proton-proton case. Therefore, the basic difference in p-nucleus collision compared to the p-p case comes from the heavier mass of the target end-point and the higher energy density of the effective firetube. The heavy target end-point, not only contributes to the enhancement of the final hadron spectra in low rapidity region, but also has as a consequence a modification of its trajectory.

As is mentioned in §II, the trajectory of an end point (mass μ) is then given by,

$$(z - z_0)^2 - (t - t_0)^2 = \left(\frac{\mu}{k}\right)^2 \tag{3.4}$$

which is a hyperbola with the center at (z_0, t_0). In the CM system of the projectile and wounded target nucleons with total energy $\sqrt{s}$, x_0 and t_0 can be chosen as,

$$x_0 = t_0 = \frac{\sqrt{s}}{2k} \tag{3.5}$$

for the end point with the mass $\mu = m_n$ and

$$x_0 = -t_0 = -\frac{\sqrt{s}}{2k} \tag{3.6}$$

for the other end point mass $\mu = M$. The hyperbolas have as asymptotes the straight lines corresponding to massless particle trajectories.

3.2 Results

In Fig.3 we show the calculated rapidity distributions dN/dy for negatively charged particles ($\bar{N}_- = \bar{N}/3$) for pp and $\alpha - p$ scatterings at 44 GeV of nucleon-nucleon CM energy, These are in excellent agreement with the experimental results[21].

In Fig.4 plotted are our rapidity distributions of $p - Ar$ and $p - Xe$ reactions for 200 GeV incident energy. In both cases a quite good agreement to the experimental data[10] was obtained except for $y < -5$, i.e, in the target fragmentation region.

Fig.5 shows the ratio,

$$R_{\alpha,p}(y) = (dN/dy)_{\alpha-p} \;/\; (dN/dy)_{p-p} \quad . \tag{3.6}$$

The rise of $R_{\alpha,p}$ at the target fragmentation region in our model comes essentially from the decay of the heavy end-point fireball. Since the mass of this end-point fireball is essentially proportional to the mean number of wounded target nucleons, we expect that the rise to be more pronounced for heavier target nuclei, as we can see in Fig.6. In all cases, our model well reproduces the trends of the experimental curves except for the sudden fall-down behavior of $p - Xe$ data in the projectile fragmentation region.

The assumption of additivity of firetube energy densities can also be extended to the nucleus-nucleus collisions. In this case, several effective firetubes with high energy density appear connecting two heavy massive end-points. Depending on the collision density we may naturally be led to the formation of local QGP like phase, since a firetube of large radius may be equivalent to a QGP plasma. However, in such cases, the fragmentation scheme of these thick firetubes is expected to be more complicated than the simple one dimensional scheme assumed here and the direct application of our model becomes questionable.

On the other hand, for collisions between light nuclei as the alpha-alpha case where the firetubes are expected to be not so thick, we still may apply our model. In Fig.7 we compare our results for $\alpha - \alpha$ scattering with the experimental data[21] where again a nice agreement is obtained. We also plotted, in Fig.5, the ratio $R_{\alpha,\alpha}(y)$. The rises of $R_{\alpha,\alpha}(y)$ both in the target and projectile fragmentation regions are well reproduced. It is interesting to note that

the relative occurence of a thick firetube with heavy mass cluster in both end-points is not negligible (see Table 1).

TABLE I. Percentage of relative occurence of firetubes with various end-point clusters. The first two columns indicate the number n_1 and n_2 of wounded nucleons in the two end-points. The numbers in the last column represent the percentual relative occurence P (%) of such firetubes.

n_1	n_2	P (%)
1	1	0.386
1	2	0.200
2	3	0.122
1	3	0.100
3	3	0.081
2	2	0.069
3	4	0.057
4	4	0.045
2	4	0.024
1	4	0.008

IV. Discussion

As mentioned in the Introduction, hadron-nucleus collisions offer an interesting possibility of studying the dynamics of multiple scattering processes of strongly interacting particles. The advantage of the firetube model is that it unifies the microscopic QCD-inspired process (formation of firetube) and the macroscopic nature of hadronization process in a simple phenomenological description. In other words, it represents a hybrid nature of string model and hydrodynamical aspects. For proton-proton collisions, the energy dependence of inclusive spectra were successfully reproduced for a very wide energy region. The direct application of this model to hadron-nucleus collisions, based on the assumption of additivity of individual nucleon-nucleon firetubes, is seen to be consistent with available experimental data. In particular, the behaviour of rapidity spectra in the projectile fragmentation region is well reproduced. The ratio $R(y)$ in this region is of the order of unity. In our model, this behavior comes from the single nucleon-nucleon collision near the nuclear edge. Consequently, the dependence of the total yield of particles at large longitudinal momentum (i.e., $x_F \sim 1$) as a function of target mass number should behave asymptotically as $A^{1/3}$ for large A, which is in fact the case for observed data[22]. However, the $p - Xe$ data show an abrupt fall-down of rapidity ratio for high y, which can not be explained by any existing model.

In the target fragmentation region the calculated rapidity spectra for heavier target shows a substancial difference from the experimental data where the latter present a peak which appears at the target rapidity ($y \simeq -3$) and then falls off rapidly for $y < -5$. This discrepancy may be attributed to the following two mechanisms which are not taken into account in the present calculation. First, the target wounded nucleons further scatter inside the nucleus causing an intranuclear cascading process among the rest of target nucleons. Second, the hadrons produced by the fireball decay at the target fragmentation region will be reabsorbed by the target nucleus. Both processes will lead to an excitation of the target nucleus followed by emission of particles via evaporation process. Further studies on this point are now in progress.

ACKNOWLEDGEMENTS

The authors are grateful to Dr.N.Prado and Prof. Y.Hama for stimulating discussions. This work was in part supported by **FINEP and CNPq** of Brasil.

Figure Captions

Fig.1 Average transverse momentum $< P_T >$ for proton-proton collisions. Solid circles are the experimental data of Refs. 18,19 and 20. The solid line represents our calculations.

Fig.2 Firetube formation between the incident nucleon and a massive object formed by de ν wounded nucleons in the target.

Fig.3 Rapidity distrinbutions for $p-p$ and α-p collisions at $\sqrt{s_{nn}}$=44 GeV. The solid curves represent our calculations for $p-p$ and $\alpha-p$. Solid and open circles are corresponding experimental data[21].

Fig.4 Same as Fig.4 for p-p, p-Ar and p-Xe reactions at proton incident energy 200 GeV. Data are taken from Ref. 10.

Fig.5 Ratios $R_{\alpha,p}$(y) and $R_{\alpha,\alpha}$(y). The solid curves represent our calculations for $R_{\alpha,p}$ and $R_{\alpha,\alpha}$. Solid and open circles are corresponding experimental data[21].

Fig.6 Same as Fig.5 for ratios $R_{p,Ar}$(y) and $R_{p,Xe}$(y). Data are taken from Ref. 10.

Fig.7 Rapidity distribution for $\alpha-\alpha$ collisions at $\sqrt{s_{nn}}$=30 GeV (solid curve). Data[21] are shown in solid cirles. For comparison, $p-p$ spectra are also shown in solid curve with the data (open circles).

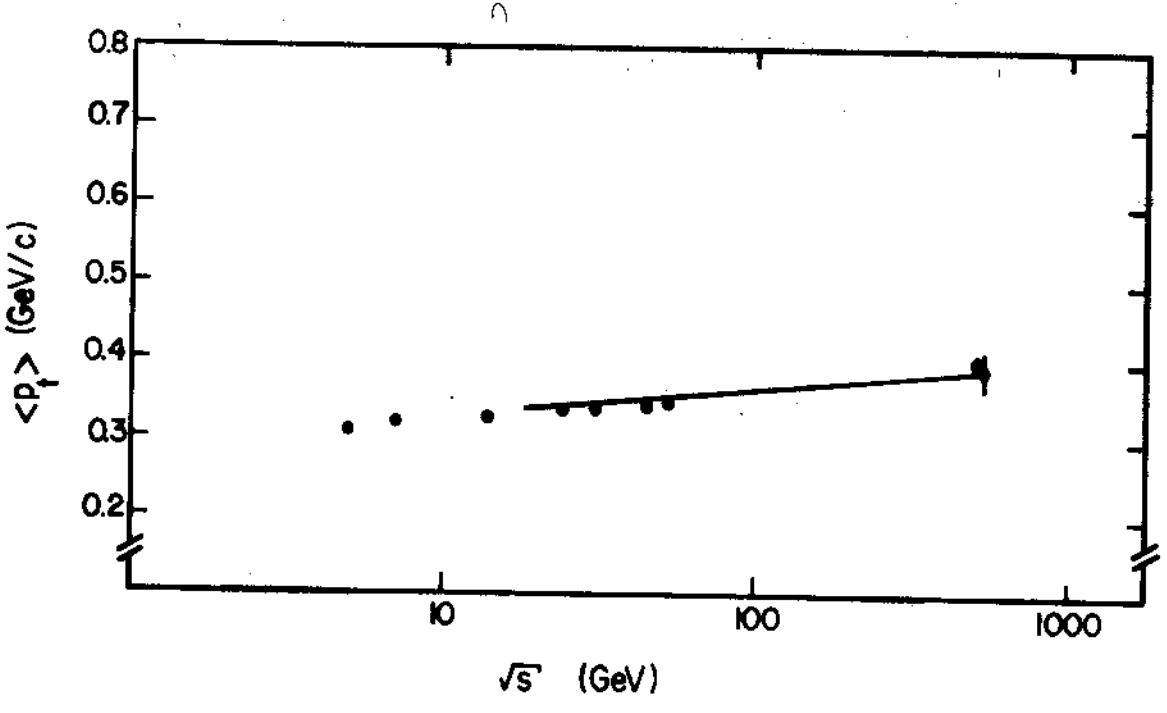

Fig. 1

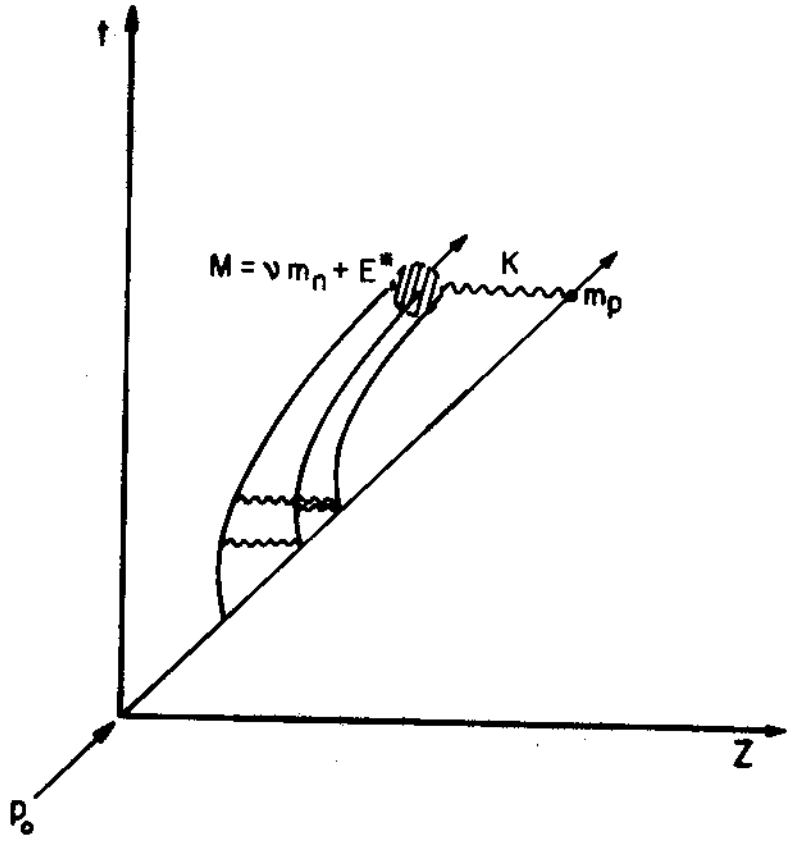

Fig. 2

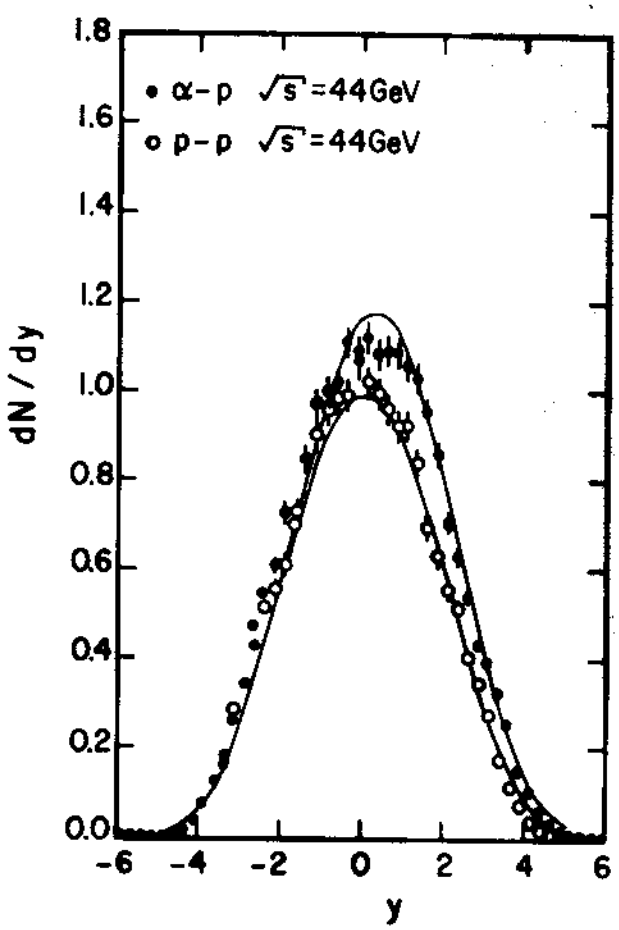

Fig. 3

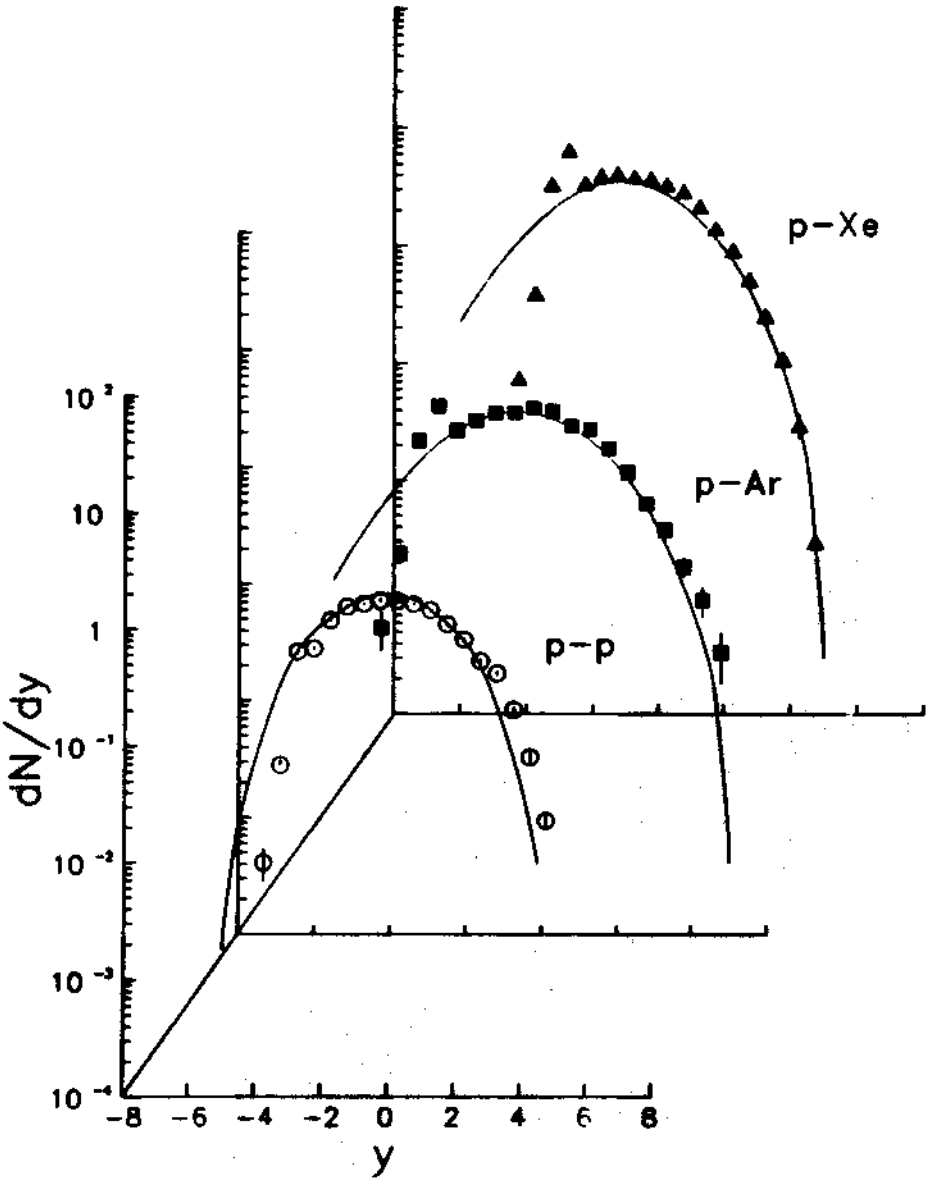

Fig. 4

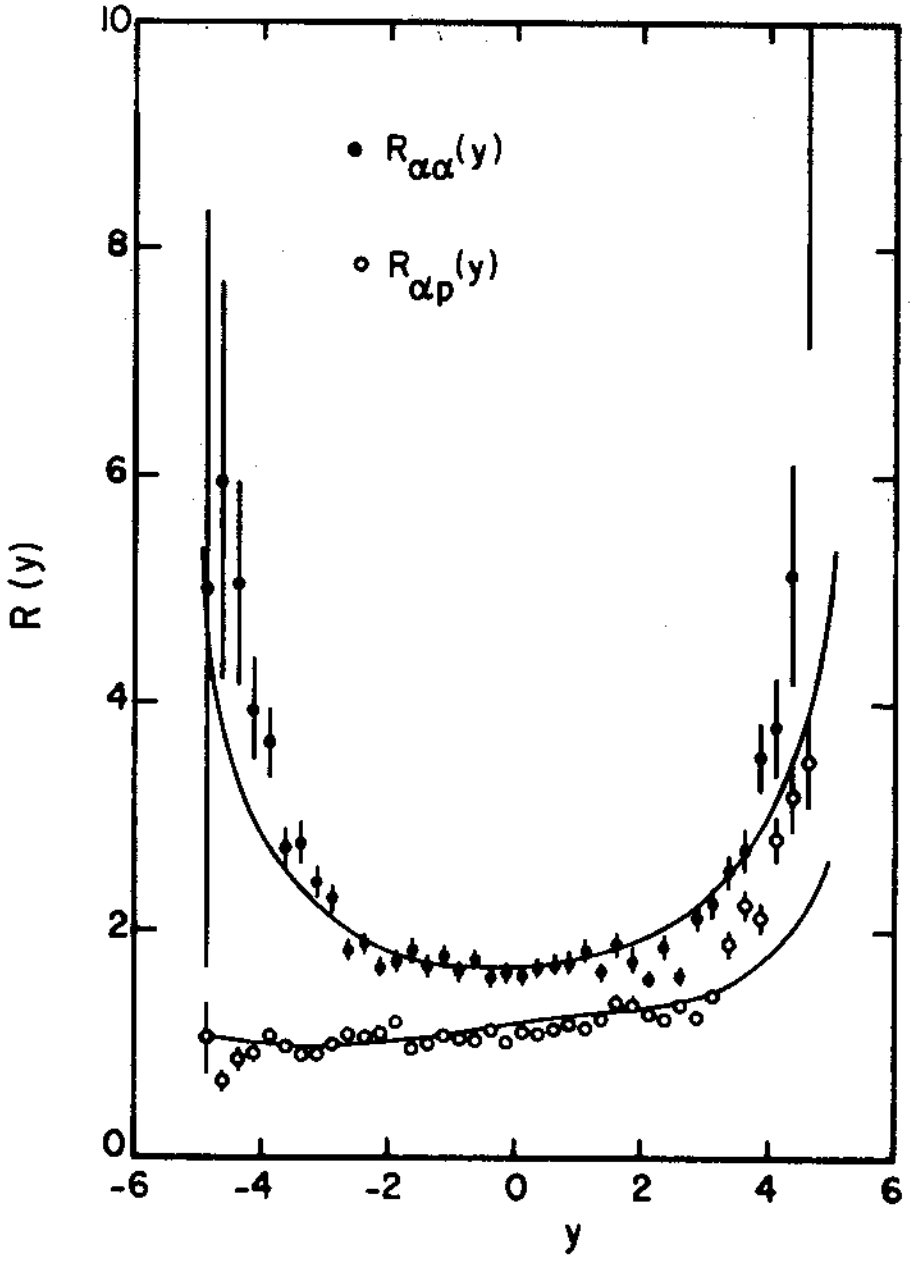

Fig. 5

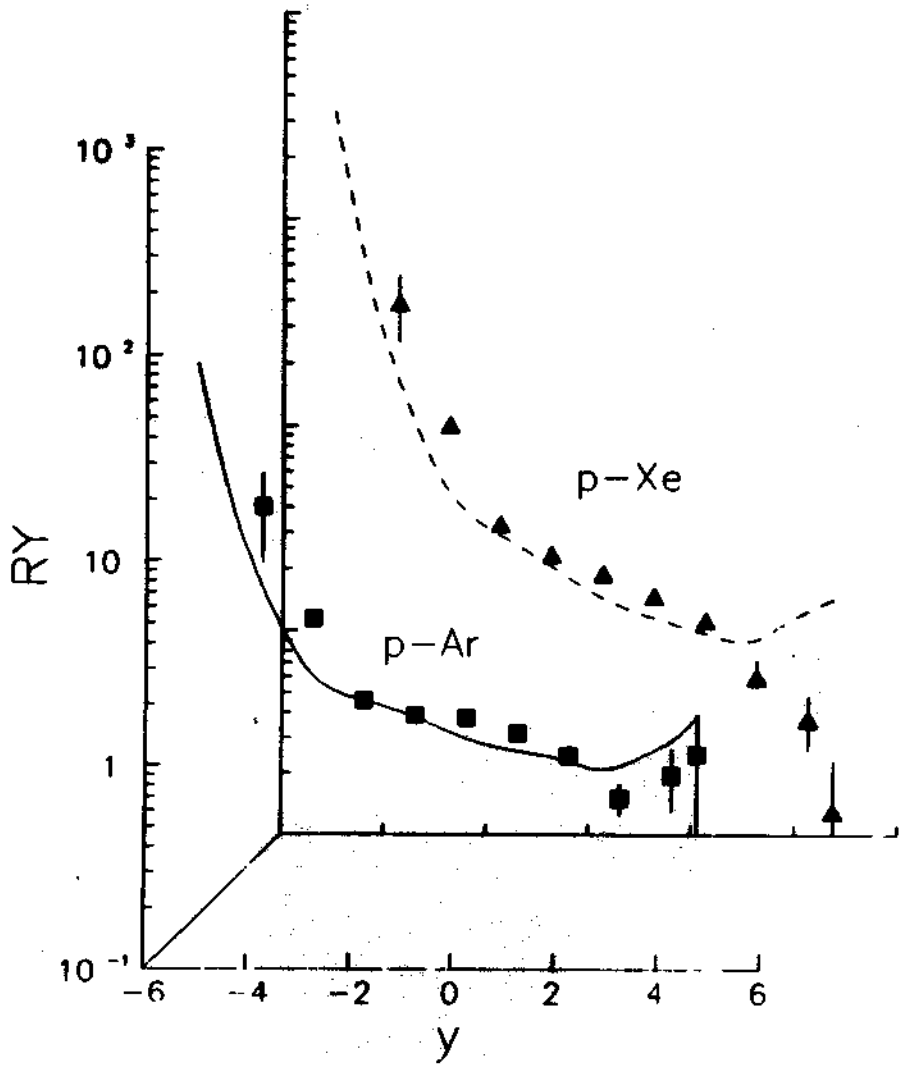

Fig. 6

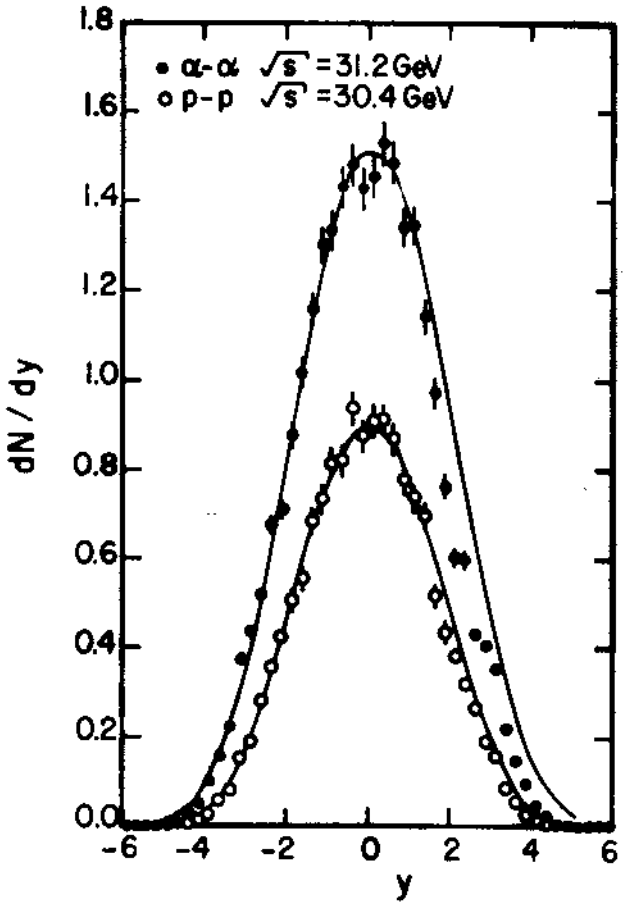
• α-α √s =31.2GeV
○ p-p √s =30.4 GeV
dN / dy
y
1.8
1.6
1.4
1.2
1.0
0.8
0.6
0.4
0.2
0.0
-6
-4
-2
0
2
4
6

Fig. 7

References

1. Proceedings of the Fifth International Conference on Ultrarelativistic Nucleus-Nucleus Collisions, Asilomar, California, 1987, edited by L. Schroeder and M. Gyulassy, Nucl. Phys. *A*461 (1987).
2. Proceedings of the Sixth International Conference on Ultrarelativistic Nucleus-Nucleus Collisions, Quark Matter 1987, Schloss Nordkirchen, Z. Phys. C.
3. in Ref. 1.
4. J. Ranft, Phys. Rev. *D*37, 1842 (1988).
5. B. Andersson, G. Gustafson, B. Nielsson-Almquist, Nucl. Phys. *B*281, 289 (1987).
6. K. Werner, Phys. Rev. *D*39, 780 (1989).
7. A. Capella, T. A. Casado, C. Pajares, A. V. Ramello and J. Tran Thanh Van, Z. Phys. *C*33, 541 (1987).
8. M. Gyulassy, preprint CERN-Th 4794/87; Proceedings of the International Conference on Intermediate Energy Nuclear Physics, Balaton-fured, Hungary (1987).
9. J. E. Elias et al., Phys. Rev. *D*22, 13 (1980).
10. C. De Marzo et al., Phys. Rev. *D*26, 1019 (1982).
11. N. Prado, R. A. M. S. Nazareth, and T. Kodama, Rev. Bras. Fis. 16, 452 (1986).
12. N. Prado, Ph.D. Thesis, Institute of Physics, UFRJ (1989).
13. R. A. M. S. Nazareth, N. Prado and T. Kodama, Phys. Rev. *D*40, (1989).
14. X. Artru and G. Mennesier, Nucl. Phys. *B*70, 93 (1971); B. Andersson, G. Gustafson, G. Ingelman, T. Sjöstrand and X. Artru, Phys. Rev. 97, 31 (1983).
15. A two-step mechanism was also suggested for $e - \bar{e}$ jet phenomena by T. D. Gottschalk, Nucl. Phys. *B*239, 349 (1984).
16. Y. Hama, Phys. Rev. *D*19, 2623 (1979).
17. G. A. Kilekhin, Zh. E.T.F. 35, 1185 (1958).
18. A. M. Rossi et al., Nucl. Phys.*B*84, 269 (1975).
19. UA2 Collaboration, M. Banner et al., Phys. Lett. *B*122, 322 (1983).
20. UA5 Collaboration, G. J. Alner et al., Phys. Rep.154, 247 (1987).
21. W. Bell et al., Z. Phys.*C*27, 191 (1985).
22. S. J. Brodsky and P. Hoyer, Phys. Rev. Lett.63, 1566 (1989).